Surface Functionalization with (3-Glycidyloxypropyl)trimethoxysilane (GOPS) as an Alternative to Blending for Enhancing the Aqueous Stability and Electronic Performance of PEDOT:PSS Thin Films

Peter O. Osazuwa,¹ Chun-Yuan Lo,² Xu Feng,² Abigail Nolin,¹ Charles Dhong,^{1,3} and Laure V. Kayser^{1,2*}

Department of Materials Science and Engineering, University of Delaware, Newark, DE, 19716, USA
Department of Chemistry and Biochemistry, University of Delaware, Newark, DE, 19716, USA
Department of Biomedical Engineering, University of Delaware, Newark, DE, 19716, USA

*Author to whom correspondence should be addressed: lkayser@udel.edu

Keywords: organic bioelectronics; water stability; PEDOT:PSS; GOPS; surface functionalization; organic electrochemical transistor

ABSTRACT

Organic mixed ionic-electronic conductors. such poly(3,4ethylenedioxythiophene):poly(styrene sulfonate) (PEDOT:PSS), are essential materials for the fabrication of bioelectronic devices due to their unique ability to couple and transport ionic and electronic charges. The growing interest in bioelectronic devices has led to the development of organic electrochemical transistors (OECTs) which can operate in aqueous solutions and transduce ionic signals of biological origin into measurable electronic signals. A common challenge with OECTs is maintaining the stability and performance of the PEDOT:PSS films operating under aqueous conditions. Although the conventional approach of blending the PEDOT:PSS dispersions with a crosslinker such as (3-Glycidyloxypropyl)trimethoxysilane (GOPS) helps to ensure strong adhesion of the films to device substrates, it also impacts the morphology and thus electrical properties of the PEDOT:PSS films which leads to a significant reduction in the performance of OECTs. In this study, we instead only functionalize the surface of the device substrates with GOPS to introduce a silane monolayer before spin-coating the PEDOT:PSS dispersion on the substrate. In all cases, having a GOPS monolayer instead of a blend leads to increased electronic performance metrics, such as three times higher electronic conductivity, volumetric capacitance, and mobilitycapacitance product $[\mu C^*]$ value in OECT devices, ultimately leading to a record value of 406 \pm 39 F cm⁻¹ V⁻¹ s⁻¹ for amorphous PEDOT:PSS. This increased performance does not come at the expense of operational stability, as both the blend and surface functionalization show similar performance when subjected to pulsed gate bias stress, long-term electrochemical cycling tests,

and aging over 150 days. Overall, this study establishes a novel approach to using GOPS, as a surface monolayer instead of a blended crosslinker, for achieving high-performance organic mixed ionic-electronic conductors that are stable in water for bioelectronics.

INTRODUCTION

The increasing demand for advanced diagnostic and therapeutic systems has facilitated the development of wearable and implantable bioelectronics for personalized health monitoring and point-of-care diagnosis. Amongst organic electronic devices used for bioelectronics, organic electrochemical transistors (OECTs) have shown significant promise due to their numerous advantages over other organic thin film transistors. OECTs can achieve over a 100-fold higher transconductance leading to higher sensitivity, decreased mechanical mismatch with biological tissues, and low operation voltage. Because of these features, OECTs have been used in bioelectronics for neuromorphic devices, to record physiological signals when interfacing biological tissues, and chemical sensing. In most cases, OECTs operate in aqueous electrolytes, such as body fluids or aqueous salt solutions, which means that the device and materials need to be mechanically and electronically stable in aqueous environments. I4-17

In the active channel of OECTs are organic materials that display mixed ionic-electronic conductivity, such as doped poly(3,4-ethylenedioxythiophene) complexed with poly(styrene sulfonate) (PEDOT:PSS) sold as a 1.3 wt% aqueous dispersion (e.g., Clevios PH1000). Owing to the ability of PEDOT:PSS to transport both ionic and electronic charges, its high capacitance and ease of processing via solution spin-coating or printing, it is the most commonly used active channel material in OECTs. While PEDOT:PSS is the material of choice for OECT channels, it cannot be used in its pristine form because PEDOT:PSS films are prone to redispersion and delamination from substrates in aqueous environments. ^{18,19} To improve the water stability of PEDOT:PSS films for applications in optoelectronics and bioelectronics, several approaches have been reported, including blending with small molecule additives, ^{20,21} nanoparticles and photocrosslinkers, ^{22,23} and the use of polymeric adhesive layers. ^{24,25} For OECTs, where PEDOT:PSS films are subjected to the stress of repetitive cation injection and extraction, due to electrochemical doping and de-doping, mechanical stability is even more challenging. Films that are not sufficiently stable result in reduced device performance over time, as measured by a decrease in transconductance in OECTs or charge storage capacity under repeated cyclic voltammetry (CV)

cycles.^{17,26} In most studies, this stability issue is addressed by blending chemical crosslinkers with the aqueous dispersions of PEDOT:PSS before the deposition of thin films. For example, blending with (3-Glycidyloxypropyl)trimethoxysilane (GOPS) (**Figure 1a**) at an optimal concentration of 1 wt%²⁷ has been widely used to enhance the operational stability of PEDOT:PSS films in OECT devices^{10,11,28–31} via the reaction of the epoxy ring moiety of GOPS with the sulfonate group of PSS, and anchoring to the substrate (e.g., glass) via a silane bond formation (**Figure 1b**).¹⁸ However, the addition of GOPS significantly decreases the conductivity¹⁸ and volumetric capacitance^{32,33,15} of PEDOT:PSS due to the formation of insulating oligo/polysiloxane chains entangled with PEDOT:PSS chains. A similar effect was also reported for PEDOT:DBSA blended with GOPS.¹⁹ Alternative crosslinkers such as poly(ethylene glycol)diglycidyl ether (PEGDE)^{34,35} and divinylsulfone (DVS)³⁶ have been explored to attain water-stable PEDOT:PSS films while

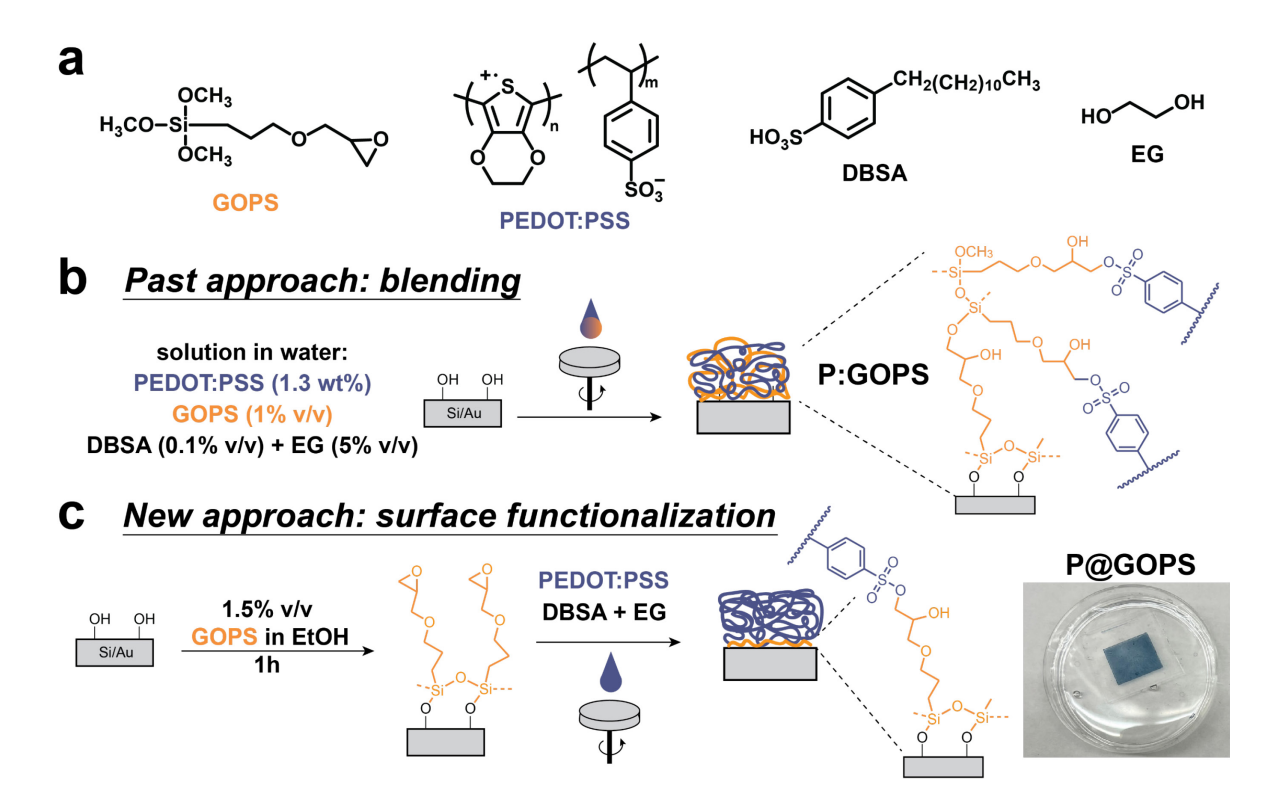


Figure 1. Overview of the two approaches used in this study to enhance the water stability of PEDOT:PSS. (a) Chemical structures of 3-glycidoxy propyltrimethoxysilane (GOPS), PEDOT:PSS, dodecylbenzene sulfonic acid (DBSA), and ethylene glycol (EG) (Left to Right). Schematic illustration of the fabrication of PEDOT:PSS films and crosslinking mechanism via (b) blending PEDOT:PSS with GOPS (P:GOPS) and (c) surface functionalization with GOPS before deposition of PEDOT:PSS (P@GOPS) (inset: picture of a P@GOPS film immersed in water).

maintaining their electronic and ionic conductivity. However, in the absence of GOPS, PEGDE and DVS crosslinked PEDOT:PSS thin films were shown to delaminate from substrates.^{36,37} This lack of aqueous stability can be explained by the absence of silane anchoring groups to maintain adhesion onto the substrates. Sulfuric acid-assisted crystallization of PEDOT:PSS via the removal of large amounts of PSS/PSSH has also been used to enhance the stability of PEDOT:PSS utilized under aqueous conditions for 21 days.¹⁵ However, sulfuric acid is a strong acid that can cause damage to flexible substrates, thus it is not suitable for the fabrication of flexible bioelectronic devices.

Herein, we report an approach to achieve PEDOT:PSS films stable in aqueous electrolytes without compromising their electronic and ionic conductivity, and overall electronic performance in OECTs. Instead of blending GOPS with PEDOT:PSS, only the surface of the substrate is functionalized with GOPS, to introduce a silane monolayer with epoxy groups before spin-coating PEDOT:PSS (Figure 1c). GOPS is commonly utilized in biomedical applications as an adhesive monolayer for the immobilization of proteins, ³⁸ DNA, ³⁹ and cervical exfoliative cells, ⁴⁰ but these monolayers had surprisingly never been explored for the deposition of PEDOT:PSS. Films obtained by surface functionalization were compared to those obtained by blending and showed similar operational stability in water under passive conditions and electrochemical cycling. But, the surface functionalization approach led to higher transconductance in OECT devices and larger volumetric capacitance. Similar to previous works which showed that interfacial interactions can improve the adhesion of conductive polymers, ^{24,41,42} we demonstrated here that this effect extends to PEDOT:PSS films of up to 450 nm operating under aqueous conditions. Depth profiling measurements, using time-of-flight secondary ion mass spectrometry (ToF-SIMS) confirmed that the silane crosslinker formed an adhesive layer between the substrate and PEDOT:PSS, and was not present in the bulk. Further, detailed materials characterization using atomic force microscopy (AFM), X-ray photoelectron spectroscopy (XPS), and Raman spectroscopy were done to assess the effect of blending and surface functionalization with GOPS on the microstructure and molecular packing of the PEDOT:PSS films. This work provides an efficient method for the preparation of organic mixed ionic-electronic conductors films stable in aqueous environments which does not compromise the electronic properties. While this work focused on PEDOT:PSS on various substrates (glass, silicon wafer, gold), the same functionalization method could be extended to other organic semiconductors containing nucleophilic substituents that can react with

epoxides, such as carboxyl,⁴³ and amine^{38,40} functional groups, to reduce substrate delamination and increase the mechanical stability of device for bioelectronics applications in aqueous environments.

EXPERIMENTAL SECTION

GOPS surface functionalization

Before functionalization of the substrates (glass, Si wafer, and Au-sputtered glass) with GOPS, substrates were first cleaned by washing with soapy water, deionized water, acetone, and isopropanol for 10 min each in sequence followed by drying under N₂ flow. The cleaned substrates were then activated using oxygen plasma for 1 min. After the oxygen plasma treatment, the substrates were immersed in an ethanol solution of 1.5% v/v GOPS for 1 h at room temperature to form a monolayer containing epoxy functional groups on the surface. The substrates were rinsed thoroughly with ethanol to remove any excess silane and dried at 80 °C in a vacuum oven.

Preparation of PEDOT:PSS thin films

The GOPS-blended sample (P:GOPS) was prepared by blending 1% v/v GOPS with PEDOT:PSS solution (Clevios PH1000) mixed with 5% v/v ethylene glycol (EG) and 0.1% v/v dodecylbenzene sulfonic acid (DBSA), filtered using a 0.45 μm polytetrafluoroethylene filter, spin-cast onto the pre-cleaned pristine substrates and annealed at 120 °C for 30 min. To prepare the PEDOT:PSS films on GOPS-functionalized substrates (P@GOPS), the PEDOT:PSS solution (Clevios PH1000) was mixed with 5% v/v EG and 0.1% v/v DBSA, filtered using a 0.45 μm polytetrafluoroethylene filter, spin-cast onto the GOPS-functionalized substrates, and annealed at 120 °C for 30 min.

RESULTS AND DISCUSSION

The goal of the surface functionalization with GOPS before spin-coating instead of blending GOPS with the PEDOT:PSS dispersion, is to ensure the stability of PEDOT:PSS thin films in devices operating in water (e.g., OECTs), without compromising on their electronic performance. We hypothesized that the re-dispersion of PEDOT:PSS films in water in the absence of GOPS is mainly due to the interfacial delamination from the substrate (adhesive failure over cohesive failure), as seen by the large flakes of PEDOT:PSS floating in water when films are immersed in water (**Figure S1a**). Therefore, by covalently anchoring PEDOT:PSS only at the substrate interface (with a GOPS monolayer), similar stability in water should be achieved without

introducing large amounts of insulator within the bulk of the films. To test this surfacefunctionalization approach, we prepared PEDOT:PSS films by spin-coating PEDOT:PSS dispersion onto GOPS-functionalized substrates (P@GOPS) (Figure 1c) and compared them with PEDOT:PSS films obtained by blending with 1% v/v GOPS before spin-coating (P:GOPS) (Figure 1b). This latter formulation for P:GOPS was chosen as it is the most commonly used ratio of GOPS in PEDOT:PSS to ensure water stability while maintaining reasonable conductivity. 10,11,28-30 P@GOPS was immersed in water and the films remained stable without delamination or redispersion (Figure 1c inset). The P@GOPS film stability in water was further assessed over a period of 20 days and it showed no sign of delamination or redispersion (Figure S1b). This result is similar to the water stability of the PEDOT:PSS films prepared via blending for P:GOPS.¹⁸ The water stability of P@GOPS was further validated as the average thickness of its thin films increased linearly with the number of spin coatings, ranging from ~100 nm to ~420 nm despite the absence of GOPS in the PEDOT:PSS solution (Figure 2a). We also assessed the change in film thickness of both P@GOPS and P:GOPS thin films over a period of 22 days in deionized water (Figure S2a). We observed a ~10% reduction in thickness between day 0 and the next analysis day (day 3) in both P@GOPS and P:GOPS after which the thickness remained fairly constant for the remaining period of the analysis. We attribute this reduction to the removal of excess PSS in agreement with our XPS result after washing the films in deionized water (see sections below).

To examine the effect of GOPS on the electrical properties of PEDOT:PSS thin films, we determined the electronic conductivity of the thin films using four probe measurements. As shown in **Figure 2b**, the conductivity of P:GOPS $(0.06 \pm 0.01~\mathrm{S~cm^{-1}})$ was lower than pristine PEDOT:PSS (Pr-P) $(0.7 \pm 0.1~\mathrm{S~cm^{-1}})$ which is consistent with the effect of GOPS on PEDOT:PSS as previously reported. ^{18,27,44} In contrast, P@GOPS showed a comparable electronic conductivity $(1.1 \pm 0.1~\mathrm{S~cm^{-1}})$ to Pr-P $(0.7 \pm 0.1~\mathrm{S~cm^{-1}})$, similar to past reports on PH1000 films without secondary additives, ⁴⁵ thus indicating that the surface functionalization approach did not compromise the electronic conductivity of PEDOT:PSS. It should be noted that even at loadings as low as $0.1~\mathrm{wt}$ % GOPS in blends, the conductivity typically drops by one order of magnitude compared with Pr-P. ¹⁸ To further validate our approach, the conductivity of P:GOPS and P@GOPS were measured after the addition of ethylene glycol (EG) and dodecylbenzene sulfonic acid (DBSA) to their respective aqueous dispersions. The additives were added to enhance the

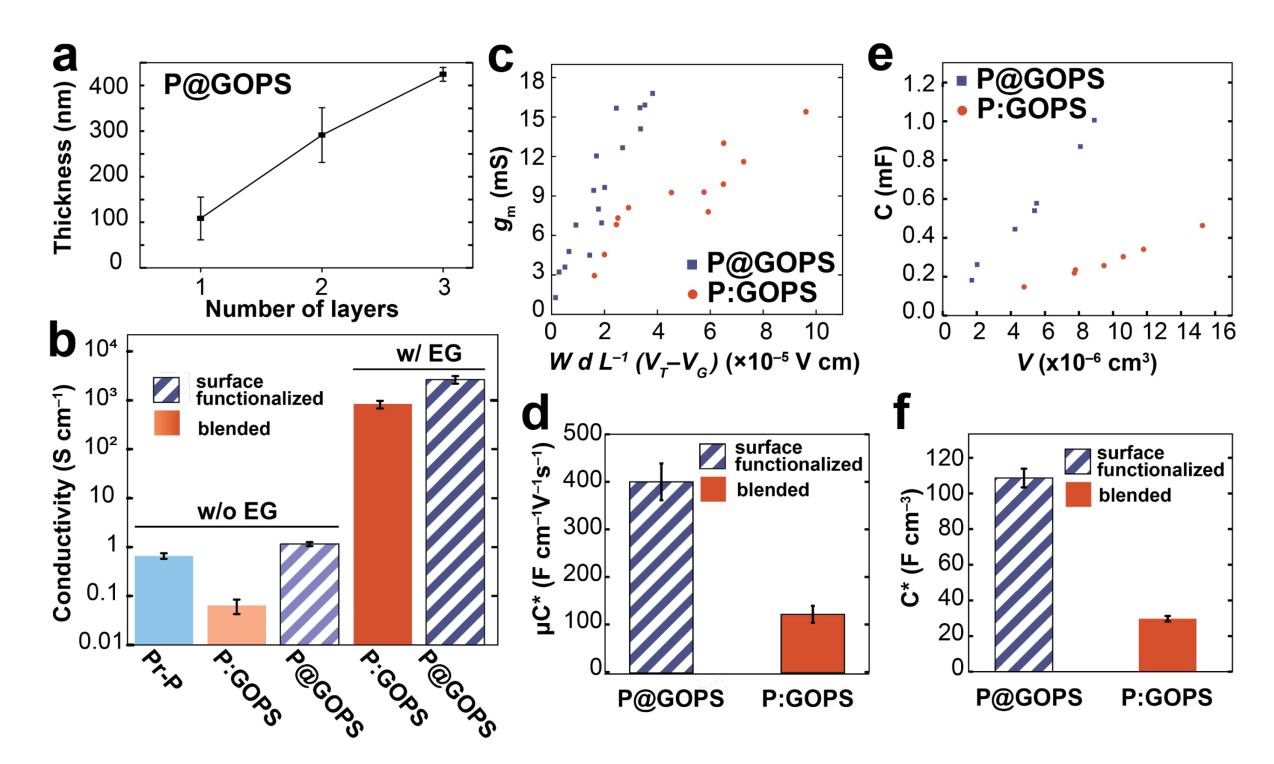


Figure 2. Electronic properties of P@GOPS and P:GOPS. (a) Film thickness as a function of the number of spin-coated layers for P@GOPS. (b) Electronic conductivity of Pr-P, P:GOPS, and P@GOPS with and without secondary dopant (EG) and DBSA. The error bars represent the standard deviation for n = 3 thin films. (c) Transconductance of P:GOPS and P@GOPS with EG as a function of applied gate potential and channel geometry. (d) Mobility-capacitance product $[\mu C^*]$ calculated from the slopes of the plots in Figure 2c. (e) Capacitance (C) as a function of film volume. (f) Volumetric capacitance (C^*) calculated from the slopes of the plots in Figure 2e.

conductivity of PEDOT:PSS and improve the quality of the thin films, respectively.⁴⁴ The additives improved the electronic conductivity of P:GOPS+EG by two orders of magnitude (826 \pm 148 S cm⁻¹) compared to Pr-P (0.7 \pm 0.1 S cm⁻¹) while a higher increase (three orders of magnitude) was obtained for P@GOPS+EG (2650 \pm 467 S cm⁻¹) compared to Pr-P (0.7 \pm 0.1 S cm⁻¹). We left the P@GOPS and P:GOPS films immersed in water over a period of 22 days and took regular conductivity measurements after drying them (**Figure S2b**). For both approaches, we observed a comparable reduction in conductivity from day 1 to 22 of approximately 30%, similar to past reports.^{46,47}

To investigate the applicability of our surface-functionalization approach as an alternative to blending for use in bioelectronics, OECT devices were fabricated with P:GOPS and P@GOPS films containing EG and DBSA additives. The OECTs were fabricated using the films as the

channel, Au as the source and drain electrodes, 0.1 M NaCl as the aqueous electrolyte, and Ag/AgCl pellet as the gate electrode. A detailed fabrication procedure is given in the supplementary information. The output characteristics (Figure S3a and S3b) and transfer curves (**Figure S3c** and **S3d**) at drain voltage, $V_D = -0.6$ V for P@GOPS and P:GOPS show that the drain current, ID decreases with gate voltage, VG, due to the injection of cations from the electrolyte which compensates the sulfonate counterions leading to a decrease in hole density in the PEDOT. This result is consistent with the common operating mechanism of OECTs. 48,49 The transfer curve also showed that both devices exhibited a similar ON/OFF ratio of ~70 for P@GOPS and ~77 for P:GOPS. The figure-of-merit that measures the effective signal amplification of an OECT is the transconductance, defined as $g_m = \partial I_D/\partial V_G$. Hence, to examine the efficiency of the P@GOPS current modulation at a given gate bias, the differential transconductance (gm) was extracted and the geometry-normalized transconductance $(g_{m,norm})$ is reported to ensure a fair comparison between devices of different channel geometries. ^{50–52} P@GOPS showed a $g_{m,norm}$ near $V_G = 0$ V of 24 ± 4 mS μm^{-1} (n = 6) which exceeded that of P:GOPS (10 \pm 1 mS μm^{-1} , n = 6). Note that the gm,norm of P@GOPS was also higher than the gm,norm of PEDOT:PSS blended with a very low concentration of GOPS (0.05 wt%) previously reported by ElMahmoudy et al.²⁷ To further assess the influence of surface functionalization, the product of the charge carrier mobility and volumetric capacitance $[\mu C^*]$ of P:GOPS and P@GOPS (Figure 2c) were calculated as it is widely accepted as the benchmark for the characterization of organic mixed conductors for OECTs and guides the design strategies for channel materials.³³ We obtained a $[\mu C^*]$ of 406 \pm 39 F cm⁻¹ V⁻¹ s⁻¹ for P@GOPS and $124 \pm 18 \text{ F cm}^{-1} \text{ V}^{-1} \text{ s}^{-1}$ for P:GOPS (**Figure 2d**). The three times higher value of μC^* suggests that GOPS surface functionalization was superior to GOPS blending for obtaining high-performance OECTs. Next, volumetric capacitance (C^*) was extracted using electrochemical impedance spectroscopy (EIS) to examine the effect of surface functionalization and blending on the magnitude of the ionic-electronic coupling per unit volume in PEDOT:PSS. 50,53 The capacitance (C) was extracted from the EIS data (Figure S4a-d) at the low-frequency region of the spectrum (0.1 to 1 Hz), where the applied alternating current amplitude modulation is slow enough for the ions to populate the film. As shown in Figure 2e, C scaled linearly with the film volume of varying geometries, and the C^* was extracted from the slope of the curve, yielding a value of 109 ± 5 F cm⁻³ for P@GOPS which was about three times higher than P:GOPS (30 ± 1 F cm⁻³, Figure 2f). Since the origin of the volumetric capacitance of PEDOT:PSS is linked to the

displacement of holes by cations,⁵³ the capacitance is correlated with the charge carrier concentration. 54,55 The hole densities can thus be estimated as the amount of charge stored per unit volume, at a potential where the volumetric capacitance of PEDOT:PSS is approximately constant, in an approach previously used by Salleo and coworkers (Equation S4).⁵⁴ Using the potential difference between the direct current potential from EIS measurements (E_{dc}, 0 V vs. Ag/AgCl) and the oxidation onset of PEDOT:PSS (~ -0.9 V vs. Ag/AgCl),²⁸ the estimated hole density of P@GOPS (6.1 \times 10²⁰ cm⁻³) was found to be about three times higher than the hole density of P:GOPS (1.9 × 10^{20} cm⁻³). However, the comparable saturation mobility ($\mu_{OECT, sat}$) of P@GOPS $(2.5 \pm 0.9 \text{ cm}^2 \text{ V}^{-1} \text{ s}^{-1}, \text{ n} = 5)$ and P:GOPS $(3.1 \pm 0.4 \text{ cm}^2 \text{ V}^{-1} \text{ s}^{-1}, \text{ n} = 5)$ extracted from the slope of $I_D^{1/2}$ vs V_G plots (**Figure S4e** and **S4f**) suggested that hole mobility was not influenced by GOPS crosslinking in the PEDOT:PSS thin films. This observation is similar to that of Stavrinidou et al. 56 who concluded that the hole mobility of PEDOT:PSS is not affected by the presence of GOPS in the films; which they determined by directly measuring the transient drift current dominated by hole transport at t = 0 s and by analyzing the response of OECTs at constant gate current. Overall, we found that the absence of crosslinked GOPS in the bulk of the PEDOT:PSS films in P@GOPS OECTs mainly resulted in an increase in the volumetric capacitance ($\sim 3x$ C^*) and in the mobility capacitance-product ($\sim 3x \left[\mu C^*\right]$). In the dry state, we also saw a $\sim 3x$ increase in conductivity, but in OECTs the charge carrier mobility remained essentially the same. Since conductivity is the product of charge carrier mobility, density and elemental charge ($\sigma = \mu pe$), our results suggest that the charge carrier density plays the dominant role in explaining differences in conductivity and OECT performance between P:GOPS and P@GOPS, similar to what others have observed. 32,57

To determine the origin of the difference between P:GOPS and P@GOPS observed during the electronic measurements, we analyzed the chemical composition and morphology of the films. The interaction between GOPS and PEDOT:PSS as well as the chemical composition of P:GOPS and P@GOPS was determined using X-ray photoelectron spectroscopy (XPS) measurements. The S2p core-level spectra of PEDOT:PSS (**Figure 3a** and **S5a**) in the range of 162–172 eV were fitted with the Lorentzian-Gaussian function to account for the S2p_{1/2} and S2p_{3/2} contributions of each S2p peak. The spectral signature of PEDOT (162–167 eV) is represented by S2p doublets with a broad asymmetric tail that extends to higher binding energies due to the positive charge of PEDOT⁺ delocalized over several adjacent chains.⁵⁸ The PSS S2p core level (167–172 eV) showed a broader peak as it accounts for the sulfur atoms in neutral PSSH and in charged PSS⁻.⁵⁸ The peak

deconvolution showed a shift (1 eV) toward high binding energies in the S2p core level of PSS for P:GOPS thin films which indicates that there was a significant interaction between GOPS and the sulfonate groups of PSS. In contrast, the S2p core level position of PSS in P@GOPS remained unchanged compared to the Pr:P thin films. Furthermore, P@GOPS film had a lower PSS:PEDOT ratio (~2.2:1) compared to P:GOPS films (~2.9:1). As the films were not immersed in water before the measurements, we believe that some excess PSS was removed from P@GOPS during the spincoating process due to the absence of GOPS crosslinker in its formulation.⁵⁹ But, since the devices operate in water and were washed by immersion in water before electronic characterization, we also performed XPS measurements after immersing the films for 2 h in deionized water (Figure 3a and S5b). After washing, we obtained a highly reduced PSS:PEDOT ratio of ~1.5:1 for P@GOPS compared to P:GOPS (~2.4:1). Note that the pristine PEDOT:PSS (Clevios PH1000) used in this study is known to have a PSS:PEDOT ratio of 2.5:1 and we obtained an experimental value of ~2.4:1 for Pr-P which supports the accuracy of our measurement. From XPS, we also measured the degree of PEDOT oxidation in P:GOPS and P@GOPS, by quantifying the ratio of PEDOT to PSS⁻ counter ions based on their S2p contributions. ^{60,61} We found that the level of oxidation was 28.5% in P:GOPS and 39.9% in P@GOPS. This result supports our electronic measurements indicating that the charge carrier density is higher in P@GOPS than in P:GOPS. To further confirm this difference in oxidation level, Raman spectra of P:GOPS and P@GOPS were recorded (**Figure 3b**). The broad band between 1370 and 1490 cm⁻¹ corresponds to the C_{α} = C_{β} symmetric stretching of the five-membered thiophene ring on the PEDOT chains. 62 In P:GOPS, this band was narrower and shifted by 6 cm⁻¹ toward higher wavenumbers compared with Pr-P and P@GOPS. This shift is indicative of a transition from a more linear quinoid (oxidized PEDOT⁺) conformation to a more coiled benzoid (neutral PEDOT⁰) conformation, i.e., a decreased concentration of PEDOT⁺ charge carriers.^{63–65,28,62} This result implies that blending PEDOT:PSS with GOPS reduces the oxidation level of PEDOT in agreement with our XPS data and previously published results.⁶⁵ Combined results from XPS and Raman spectroscopy point towards the presence of a significant fraction of dedoped PEDOT in P:GOPS which explains the decrease in charge carrier concentration and reduced electronic performance in P:GOPS blends compared to P@GOPS.

The relative distribution of PEDOT:PSS and GOPS across the depths of the thin films were also investigated via depth-profiling studies with a time-of-flight secondary ion mass spectrometry (ToF-SIMS). We used the PSS fragment (C₈H₇SO₃⁻) as the marker for identifying the PEDOT:PSS component. Due to the similarities in the secondary ion fragments from GOPS and PEDOT:PSS, we used the Si⁻ ion for the identification of GOPS as well as the Si substrate. The depth profile in sputter time (**Figure S5c**) was transformed to a depth scale (**Figure 3c**) using the sputtering rates of each sample calculated from the sputter time and film thickness. ToF-SIMS showed that PEDOT:PSS was evenly distributed across the depth of all three films up to the film-Si substrate interface of P:GOPS (1 layer ~110 nm), P@GOPS (3 layers ~130 nm) and Pr-P (1 layer ~61 nm) where the intensity of PEDOT:PSS (C₈H₇SO₃⁻) fell while that of Si⁻ rose and later stabilized due to continued sputtering into the silicon wafer substrate. The depth profile of P@GOPS showed that, in contrast with P:GOPS, the intensity of PEDOT:PSS remained higher than GOPS across

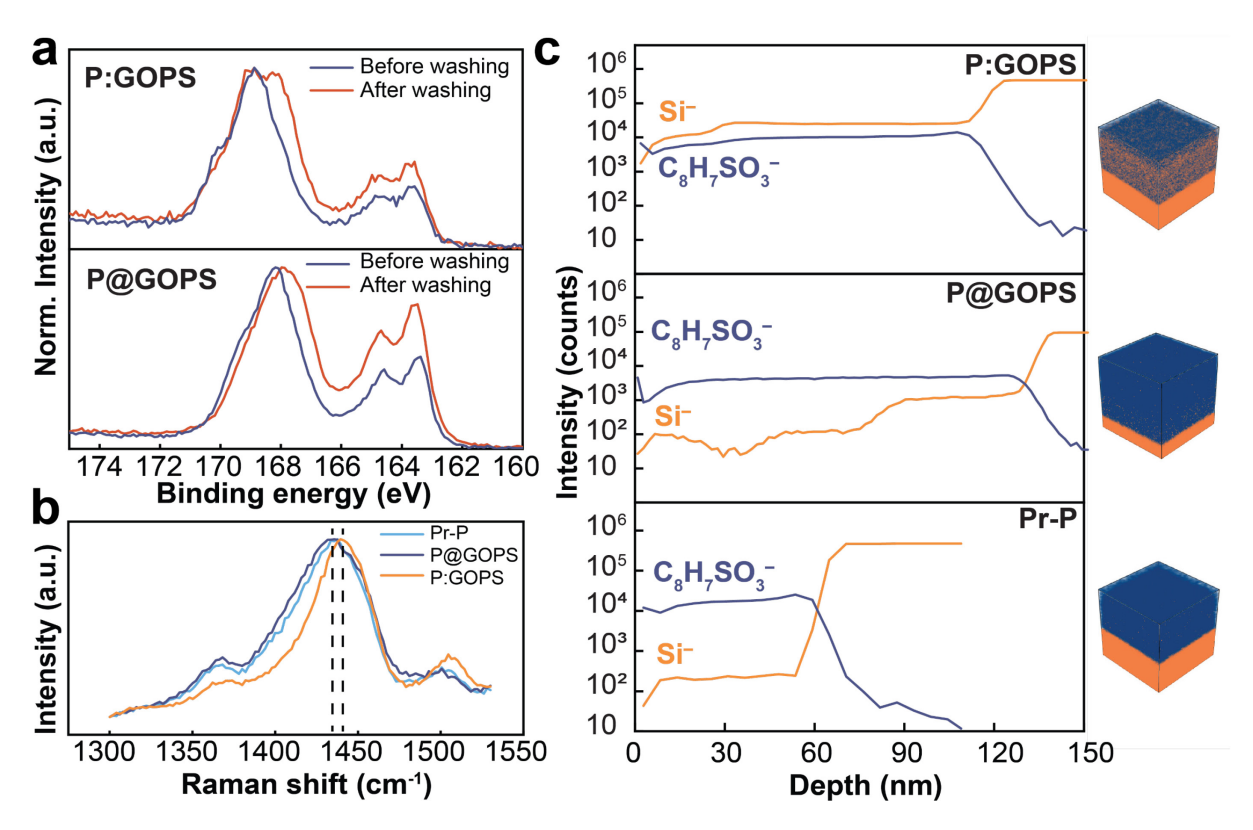


Figure 3. Surface and bulk chemical composition of the PEDOT:PSS films. (a) XPS S(2p) spectra of P:GOPS (top) and P@GOPS (bottom) before and after washing with deionized water. (b) Raman spectra in the PEDOT regio. (c) Depth profiles and 3D view obtained by ToF-SIMS of C₈H₇SO₃⁻ (dark blue) and Si⁻ (orange) ions for P:GOPS, P@GOPS, and Pr-P.

the depth of the film. It is interesting to note that the layer closest to the silicon wafer (first spincoated and showing between (~90 nm and ~130 nm) had a slightly higher intensity of Si⁻. Then, the intensity dropped to similar levels as in Pr-P. This results implies that there may be a slight diffusion of GOPS in the layer closest to the interface, but essentially none for subsequent layers. Similar to what was observed with the profilometer, these depth profiles also showed that the P:GOPS films were significantly thicker than the P@GOPS thin films as it required three layers of spin coating to reach a similar thickness of P:GOPS; simply due to the presence of added materials (i.e., oligo/polysiloxane chains from crosslinked GOPS) in the P:GOPS film. The results from the ToF-SIMS analysis are noteworthy when considering that the formulation of pristine PEDOT:PSS (Clevios PH1000) has a solid content of 1.0 to 1.3 wt% in water. Thus, blending pristine PEDOT:PSS with 1% v/v GOPS results in a film formulation with an almost equal amount of PEDOT:PSS and GOPS (~double the film thickness). In other words, the concentration of PEDOT, and by extension the density of possible charge carriers, in P:GOPS blended films is approximately half that of Pr-P and P@GOPS. Combined, the XPS, Raman and ToF-SIMS experiments point towards a higher concentration of PEDOT in the P@GOPS films than in P:GOPS, and a higher density of charge carriers (quinoidal PEDOT⁺), which explain the larger volumetric capacitance and conductivity observed. 15,32,33

We were also interested in seeing whether the GOPS in the P:GOPS films made them more hydrophobic by dynamic water contact angle measurements with the sessile drop technique (**Figure S6**). These measurements showed that the film surfaces of P@GOPS and P:GOPS were similar in hydrophilicity. P:GOPS had a receding and an advancing contact angle of $(19^{\circ}-33^{\circ}) \pm 3^{\circ}$ (n = 5) while P@GOPS had a receding and an advancing contact angle of $(24^{\circ}-38^{\circ}) \pm 3^{\circ}$ (n = 5). The similar surface energy indicates that the film composition at the surface, by contact angle, is similar which suggests that both films have a similar degree of heterogeneity on their surfaces.⁶⁶

We therefore studied the difference in surface morphology between P:GOPS and P@GOPS films by atomic force microscopy (AFM). The height images of the films revealed a fiber-like surface roughness with a similar root mean square surface roughness of 1.3 ± 0.1 nm (n = 5) for P:GOPS (Figure 4a) and 1.7 ± 0.1 nm (n = 5) for P@GOPS (Figure 4c). The fibril-like morphology is consistent with that of PEDOT:PSS mixed with EG as a co-solvent. 67,68 In phase images, the bright regions are typically associated with PEDOT-rich domains (stiffer) and the darker regions to PSS-rich domains (softer).⁶⁷ The AFM phase image of P:GOPS (Figure 4b) showed a poor phase separation in which the hard PEDOT-rich domains (bright area) are mixed with the soft PSS-rich domains (dark area) and the image appears dark because of the higher PSS:PEDOT ratio in the film microstructure. This observation is in contrast to the AFM phase image of P@GOPS (Figure 4d) which showed a clear phase separation between the PEDOT-rich domains and the PSS-rich domains which led to the formation of enlarged and interconnected PEDOT domains. In addition, the enhanced phase separation between the PEDOT-rich domains and the PSS-rich domains in P@GOPS induced a higher phase shift (58°) due to the interaction between the AFM tip and the hard PEDOT-rich domains. 69-71 In comparison, the poor phase separation in P:GOPS led to a low phase shift (16°) which indicates that the interaction was

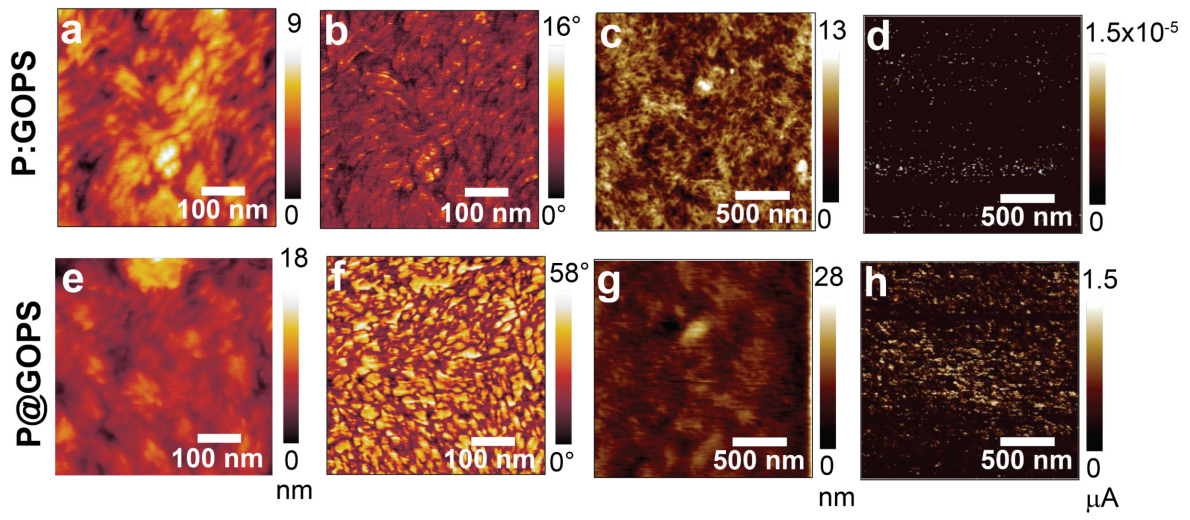


Figure 4. AFM and TUNA images of P:GOPS (top: a-d) and P@GOPS (bottom: e-h). (a and e) Height images. (b and f) Phase images. (c and g) Height images in TUNA mode. (d and h) Electrical current maps.

predominantly between the AFM tip and soft PSS/GOPS-rich domains due to the high PSS:PEDOT ratio. These morphological features suggest that the absence of GOPS in the microstructure of P@GOPS promoted the removal of insulating PSS chains and enhanced the close packing/density of PEDOT domains. The results shown here are consistent with the data obtained in the ToF-SIMS analysis and further support the idea that the lower electronic properties of P:GOPS are due to the presence of a substantial amount of GOPS in the microstructure of the PEDOT:PSS films which promotes the random distribution and isolation of the PEDOT nanofibrils leading to a decrease in the volume density of charge carriers. 15 The higher electronic properties of P@GOPS are attributed to more densely packed PEDOT-rich domains, 33,15 and the absence of hydrophobic and insulating GOPS chains in the microstructure which would facilitate ionic-electronic coupling. This effect was also confirmed by tunneling AFM (TUNA) to measure currents through the P:GOPS (Figure 4c and 4d) and P@GOPS films (Figure 4g and 4h) deposited on ITO substrates. P@GOPS showed a higher density of conductive particles with peak currents of a five orders of magnitude higher amplitude (1.5 μA for P@GOPS versus 1.5x10⁻⁵ μA for P:GOPS). For comparison, Pr-P (not washed) showed peak currents of $3.7x10^{-5}~\mu A$ (Figure S7).

To assess the suitability of P@GOPS films for practical bioelectronic applications, we evaluated the long-term performance of OECT devices made with P:GOPS or P@GOPS under several stress conditions including long-term storage in water, and repeated cation stress under OECT operation and CV. We performed an aging test by immersing the devices in 0.1 M NaCl at room temperature for 150 days and measured the transfer characteristics ($V_D = -0.6 \text{ V}$) during this period. The geometry-normalized transconductance, $g_{m,norm}$, of the devices (**Figure 5a**) was calculated from the transfer curves and showed a 56% reduction in the $g_{m,norm}$ of P@GOPS compared to a 76% reduction in the $g_{m,norm}$ of P:GOPS after 150 days. While the OECT performance of both formulations degraded over time, the $g_{m,norm}$ of P@GOPS OECT devices after 150 days (11 ± 2 mS μ m⁻¹, n = 4) in 0.1 M NaCl remained higher than the $g_{m,norm}$ of P:GOPS devices at day 1 (10 ± 1 mS μ m⁻¹, n = 4). We postulated that the significant reduction in the performance of P:GOPS is due to excessive water uptake facilitated by the higher PSS-to-PEDOT ratio in the films. This result is consistent with that of Menezes et al. who reported that absorbed water molecules can act as plasticizers which can affect the electrochemical properties of hydrated PEDOT:PSS.⁷² The current generated upon successive gate voltage pulses of +0.4 and 0 V (V_D =

-0.6 V, Δt = 1 s) was also stable for both samples over 1000 on/off cycles (2000 s) (**Figures 5c** and **5d**). Lastly, we investigated the electrochemical stability of the devices based on CV in 0.1 M NaCl. The CV curves (**Figure S8**) showed no change in charge storage capacity (CSC) of P@GOPS after 10,000 CV cycles (~ 39 h), demonstrating excellent electrochemical stability (**Figure 5b**). Furthermore, P@GOPS films remained intact without any observable interfacial failure after 10,000 charging and discharging cycles. P:GOPS films are also stable over the same range of electrochemical cycling, however, its CSC of 6 mC cm⁻² is only approximately half that of P@GOPS (11 mC cm⁻²). These results emphasize that surface functionalization of substrates is sufficient to improve the aqueous stability of PEDOT:PSS films whilst also providing a higher electronic performance under several operational conditions.

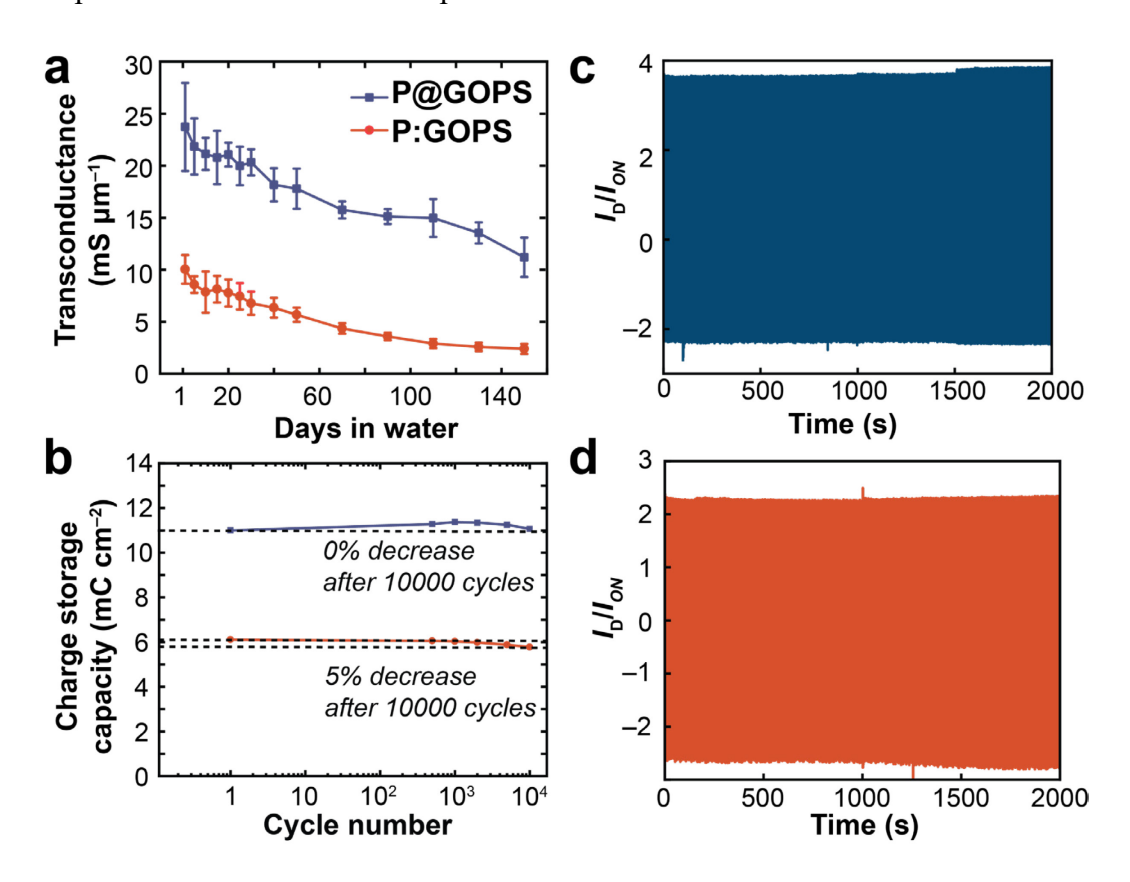


Figure 5. Stability of P@GOPS and P:GOPS films in water and under electrochemical cycling. (a) Geometry normalized transconductance as a function of aging time in an aqueous 0.1 M NaCl solutions. Error bars represent standard deviation (n = 4). (b) Charge storage capacity (CSC) over 10,000 electrochemical cycles. (c) Pulse measurements (V_G varied from 0 to 0.4 V, with a pulse length = 0.05 s, at $V_D = -0.6$ V) with over 1000 cycles of continuous operation in 0.1 M NaCl electrolyte for P:GOPS and (d) P@GOPS.

CONCLUSIONS

We demonstrated that functionalizing the surface of substrates with (3glycidyloxypropyl)trimethoxysilane (GOPS) instead of blending could be used to design highperformance and water-stable PEDOT:PSS films. The absence of GOPS in the bulk of the surface functionalized films led to a lower PSS:PEDOT ratio and enhanced phase separation between PEDOT and PSS domains, resulting in a higher charge carrier density. This microstructure in the surface-functionalized PEDOT:PSS films resulted in a larger volumetric capacitance (109 ± 5 F cm⁻³) compared to the films made from PEDOT:PSS blended with 1 wt% GOPS ($30 \pm 1 \text{ F cm}^{-3}$). In addition, OECT devices fabricated with the surface functionalized PEDOT:PSS films showed a larger geometry-normalized transconductance (10 \pm 1 mS μ m⁻¹) and higher benchmark [μ C*] value of $406 \pm 39 \text{ F cm}^{-1} \text{ V}^{-1} \text{ s}^{-1}$ compared to GOPS-blended PEDOT:PSS. Furthermore, the surface-functionalized films exhibited a comparable performance to the blended films when subjected to pulsed gate bias stress and long-term electrochemical cycling tests. However, the long-term aging test showed that the OECT devices fabricated with the surface functionalized PEDOT:PSS films have a better tolerance for storage in water as evidenced by the lower degradation (56%) in transconductance compared to 76% degradation recorded in the blended films after 150 days. We expect that this study will contribute to a further understanding of the fundamental aspects of ionic-electronic coupling and transport in organic mixed conductors. It also strengthens the case for the functionalization of substrates with GOPS instead of the conventional blending approach to minimize the content of the crosslinker in the bulk of the films, which enables water-stable films and high-performance organic mixed ionic-electronic conductors for biological interfaces.

Supporting Information

Supplementary information is available and includes the origin and purification of the materials used in this study, the OECT device fabrication and characterization, CV, EIS, four-point probe, and pulse measurement studies, and details on the acquisition of water contact angle, XPS, ToF-SIMS, Raman, AFM, and TUNA.

Authors Contributions

L.V.K. designed and supervised the project. P.O.O. performed the majority of the experiments, including the films and device fabrication, and the electronic and microstructure characterization. C.-Y.L. collected some of the AFM data, collected and analyzed the TUNA, and advised on OECT characterization, X.F. helped perform the Raman and ToF-SIMS and assisted with data analysis, A.N. and C.D. did the water contact angle measurements and analysis. L.V.K. and P.O.O. wrote the manuscript, and all the authors commented on and edited the manuscript.

Notes

The authors declare no competing financial interests.

Acknowledgments

The research reported in this publication was supported by a CAREER award from the National Science Foundation (NSF) (grant No. DMR-2237888) and start-up funds from the University of Delaware (UD) to L.V.K. We acknowledge the financial support for P.O.O. from the graduate traineeship program NRT- HDR: Computing and Data Science Training for Materials Innovation, Discovery, Analytics (MIDAS) funded by NSF grant No. 2125703. C.D. and A.N. acknowledge support from the NIH-NEI under grant No. R01EY032584-02. We thank Dr. Scott Keene for providing the Lab View code for the pulsed gate bias stress tests. We thank Dr. Lucas Flagg for insightful discussions. We thank the Surface Analysis Facility at the University of Delaware for assistance in the XPS, Raman spectroscopy, and ToF-SIMS measurements. The authors thank the DBI Bio-Imaging Center at the University of Delaware for access to the AFM instrument (NIH-NIGMS grant No. P20 GM103446, NSF grant No. IIA-1301765, and the State of Delaware). XPS analysis was performed with the instrument sponsored by the NSF under grant No. CHE-1428149. ToF-SIMS analysis was performed with the instrument sponsored by the NSF under grant No. DMR-2116754.

REFERENCES

(1) Strakosas, X.; Bongo, M.; Owens, R. M. The Organic Electrochemical Transistor for Biological Applications. *J. Appl. Polym. Sci.* **2015**, *132* (15). https://doi.org/10.1002/app.41735.

- (2) Rivnay, J.; Inal, S.; Salleo, A.; Owens, R. M.; Berggren, M.; Malliaras, G. G. Organic Electrochemical Transistors. *Nat. Rev. Mater.* **2018**, *3* (2), 1–14. https://doi.org/10.1038/natrevmats.2017.86.
- (3) Nielsen, C. B.; Giovannitti, A.; Sbircea, D.-T.; Bandiello, E.; Niazi, M. R.; Hanifi, D. A.; Sessolo, M.; Amassian, A.; Malliaras, G. G.; Rivnay, J.; McCulloch, I. Molecular Design of Semiconducting Polymers for High-Performance Organic Electrochemical Transistors. *J. Am. Chem. Soc.* **2016**, *138* (32), 10252–10259. https://doi.org/10.1021/jacs.6b05280.
- (4) Lee, W.; Kobayashi, S.; Nagase, M.; Jimbo, Y.; Saito, I.; Inoue, Y.; Yambe, T.; Sekino, M.; Malliaras, G. G.; Yokota, T.; Tanaka, M.; Someya, T. Nonthrombogenic, Stretchable, Active Multielectrode Array for Electroanatomical Mapping. *Sci. Adv.* **2018**, *4* (10), eaau2426. https://doi.org/10.1126/sciadv.aau2426.
- (5) Tropp, J.; Meli, D.; Rivnay, J. Organic Mixed Conductors for Electrochemical Transistors. *Matter* **2023**, *0* (0). https://doi.org/10.1016/j.matt.2023.05.001.
- (6) Ji, X.; Paulsen, B. D.; Chik, G. K. K.; Wu, R.; Yin, Y.; Chan, P. K. L.; Rivnay, J. Mimicking Associative Learning Using an Ion-Trapping Non-Volatile Synaptic Organic Electrochemical Transistor. *Nat. Commun.* **2021**, *12* (1), 2480. https://doi.org/10.1038/s41467-021-22680-5.
- (7) Zhang, Y.; Ye, G.; van der Pol, T. P. A.; Dong, J.; van Doremaele, E. R. W.; Krauhausen, I.; Liu, Y.; Gkoupidenis, P.; Portale, G.; Song, J.; Chiechi, R. C.; van de Burgt, Y. High-Performance Organic Electrochemical Transistors and Neuromorphic Devices Comprising Naphthalenediimide-Dialkoxybithiazole Copolymers Bearing Glycol Ether Pendant Groups. *Adv. Funct. Mater.* **2022**, *32* (27), 2201593. https://doi.org/10.1002/adfm.202201593.
- (8) Gao, D.; Parida, K.; Lee, P. S. Emerging Soft Conductors for Bioelectronic Interfaces. *Adv. Funct. Mater.* **2020**, *30* (29), 1907184. https://doi.org/10.1002/adfm.201907184.
- (9) Dimov, I. B.; Moser, M.; Malliaras, G. G.; McCulloch, I. Semiconducting Polymers for Neural Applications. *Chem. Rev.* **2022**, *122* (4), 4356–4396. https://doi.org/10.1021/acs.chemrev.1c00685.
- (10) Koklu, A.; Wustoni, S.; Musteata, V.-E.; Ohayon, D.; Moser, M.; McCulloch, I.; Nunes, S. P.; Inal, S. Microfluidic Integrated Organic Electrochemical Transistor with a Nanoporous Membrane for Amyloid-β Detection. *ACS Nano* **2021**, *15* (5), 8130–8141. https://doi.org/10.1021/acsnano.0c09893.
- Guo, K.; Wustoni, S.; Koklu, A.; Díaz-Galicia, E.; Moser, M.; Hama, A.; Alqahtani, A. A.; Ahmad, A. N.; Alhamlan, F. S.; Shuaib, M.; Pain, A.; McCulloch, I.; Arold, S. T.; Grünberg, R.; Inal, S. Rapid Single-Molecule Detection of COVID-19 and MERS Antigens via Nanobody-Functionalized Organic Electrochemical Transistors. *Nat. Biomed. Eng.* **2021**, *5* (7), 666–677. https://doi.org/10.1038/s41551-021-00734-9.

- (12) Torricelli, F.; Alessandri, I.; Macchia, E.; Vassalini, I.; Maddaloni, M.; Torsi, L. Green Materials and Technologies for Sustainable Organic Transistors. *Adv. Mater. Technol.* **2022**, 7 (2), 2100445. https://doi.org/10.1002/admt.202100445.
- (13) Xiang, H.; Li, Z.; Liu, H.; Chen, T.; Zhou, H.; Huang, W. Green Flexible Electronics Based on Starch. *Npj Flex. Electron.* **2022**, *6* (1), 1–16. https://doi.org/10.1038/s41528-022-00147-x.
- Giovannitti, A.; Nielsen, C. B.; Sbircea, D.-T.; Inal, S.; Donahue, M.; Niazi, M. R.; Hanifi, D. A.; Amassian, A.; Malliaras, G. G.; Rivnay, J.; McCulloch, I. N-Type Organic Electrochemical Transistors with Stability in Water. *Nat. Commun.* **2016**, *7* (1), 13066. https://doi.org/10.1038/ncomms13066.
- (15) Kim, S.-M.; Kim, C.-H.; Kim, Y.; Kim, N.; Lee, W.-J.; Lee, E.-H.; Kim, D.; Park, S.; Lee, K.; Rivnay, J.; Yoon, M.-H. Influence of PEDOT:PSS Crystallinity and Composition on Electrochemical Transistor Performance and Long-Term Stability. *Nat. Commun.* **2018**, 9 (1), 3858. https://doi.org/10.1038/s41467-018-06084-6.
- (16) Savva, A.; Cendra, C.; Giugni, A.; Torre, B.; Surgailis, J.; Ohayon, D.; Giovannitti, A.; McCulloch, I.; Di Fabrizio, E.; Salleo, A.; Rivnay, J.; Inal, S. Influence of Water on the Performance of Organic Electrochemical Transistors. *Chem. Mater.* **2019**, *31* (3), 927–937. https://doi.org/10.1021/acs.chemmater.8b04335.
- (17) Tang, K.; Miao, W.; Guo, S. Crosslinked PEDOT:PSS Organic Electrochemical Transistors on Interdigitated Electrodes with Improved Stability. *ACS Appl. Polym. Mater.* **2021**, *3* (3), 1436–1444. https://doi.org/10.1021/acsapm.0c01292.
- (18) Håkansson, A.; Han, S.; Wang, S.; Lu, J.; Braun, S.; Fahlman, M.; Berggren, M.; Crispin, X.; Fabiano, S. Effect of (3-Glycidyloxypropyl)Trimethoxysilane (GOPS) on the Electrical Properties of PEDOT:PSS Films. *J. Polym. Sci. Part B Polym. Phys.* **2017**, *55* (10), 814–820. https://doi.org/10.1002/polb.24331.
- Tumová, Š.; Malečková, R.; Kubáč, L.; Akrman, J.; Enev, V.; Kalina, L.; Vojtková, E.; Pešková, M.; Víteček, J.; Vala, M.; Weiter, M. Novel Highly Stable Conductive Polymer Composite PEDOT:DBSA for Bioelectronic Applications. *Polym. J.* **2023**, 1–13. https://doi.org/10.1038/s41428-023-00784-7.
- Döbbelin, M.; Marcilla, R.; Tollan, C.; Pomposo, J. A.; Sarasua, J.-R.; Mecerreyes, D. A New Approach to Hydrophobic and Water-Resistant Poly(3,4-Ethylenedioxythiophene):Poly(Styrenesulfonate) Films Using Ionic Liquids. *J. Mater. Chem.* **2008**, *18* (44), 5354–5358. https://doi.org/10.1039/B808723G.
- Jorge, S. M.; Santos, L. F.; Galvão, A.; Morgado, J.; Charas, A. Concurrent Enhancement of Conductivity and Stability in Water of Poly(3,4-Ethylenedioxythiophene):Poly(Styrenesulfonate) Films Using an Oxetane Additive. *Adv. Mater. Interfaces* **2021**, *8* (15), 2100517. https://doi.org/10.1002/admi.202100517.

- Yin, H.-E.; Huang, F.-H.; Chiu, W.-Y. Hydrophobic and Flexible Conductive Films Consisting of PEDOT:PSS-PBA/Fluorine-Modified Silica and Their Performance in Weather Stability. *J. Mater. Chem.* **2012**, *22* (28), 14042–14051. https://doi.org/10.1039/C2JM31352A.
- (23) Ha, S. R.; Park, S.; Oh, J. T.; Kim, D. H.; Cho, S.; Bae, S. Y.; Kang, D.-W.; Kim, J.-M.; Choi, H. Water-Resistant PEDOT:PSS Hole Transport Layers by Incorporating a Photo-Crosslinking Agent for High-Performance Perovskite and Polymer Solar Cells. *Nanoscale* **2018**, *10* (27), 13187–13193. https://doi.org/10.1039/C8NR02903B.
- Inoue, A.; Yuk, H.; Lu, B.; Zhao, X. Strong Adhesion of Wet Conducting Polymers on Diverse Substrates. *Sci. Adv.* **2020**, *6* (12), eaay5394. https://doi.org/10.1126/sciadv.aay5394.
- Liu, L.; Li, S.; Wu, L.; Chen, D.; Cao, K.; Duan, Y.; Chen, S. Enhanced Flexibility and Stability of PEDOT:PSS Electrodes through Interfacial Crosslinking for Flexible Organic Light-Emitting Diodes. *Org. Electron.* **2021**, *89*, 106047. https://doi.org/10.1016/j.orgel.2020.106047.
- (26) Savva, A.; Wustoni, S.; Inal, S. Ionic-to-Electronic Coupling Efficiency in PEDOT:PSS Films Operated in Aqueous Electrolytes. *J. Mater. Chem. C* **2018**, *6* (44), 12023–12030. https://doi.org/10.1039/C8TC02195C.
- ElMahmoudy, M.; Inal, S.; Charrier, A.; Uguz, I.; Malliaras, G. G.; Sanaur, S. Tailoring the Electrochemical and Mechanical Properties of PEDOT:PSS Films for Bioelectronics. *Macromol. Mater. Eng.* **2017**, 302 (5), 1600497. https://doi.org/10.1002/mame.201600497.
- (28) Keene, S. T.; van der Pol, T. P. A.; Zakhidov, D.; Weijtens, C. H. L.; Janssen, R. A. J.; Salleo, A.; van de Burgt, Y. Enhancement-Mode PEDOT:PSS Organic Electrochemical Transistors Using Molecular De-Doping. *Adv. Mater.* **2020**, *32* (19), 2000270. https://doi.org/10.1002/adma.202000270.
- (29) Rivnay, J.; Leleux, P.; Ferro, M.; Sessolo, M.; Williamson, A.; Koutsouras, D. A.; Khodagholy, D.; Ramuz, M.; Strakosas, X.; Owens, R. M.; Benar, C.; Badier, J.-M.; Bernard, C.; Malliaras, G. G. High-Performance Transistors for Bioelectronics through Tuning of Channel Thickness. *Sci. Adv.* **2015**, *1* (4), e1400251. https://doi.org/10.1126/sciadv.1400251.
- (30) Spyropoulos, G. D.; Gelinas, J. N.; Khodagholy, D. Internal Ion-Gated Organic Electrochemical Transistor: A Building Block for Integrated Bioelectronics. *Sci. Adv.* **2019**, *5* (2), eaau7378. https://doi.org/10.1126/sciadv.aau7378.
- (31) Lo, C.-Y.; Wu, Y.; Awuyah, E.; Meli, D.; Nguyen, D. M.; Wu, R.; Xu, B.; Strzalka, J.; Rivnay, J.; Martin, D. C.; Kayser, L. V. Influence of the Molecular Weight and Size Distribution of PSS on Mixed Ionic-Electronic Transport in PEDOT:PSS. *Polym. Chem.* **2022**, *13* (19), 2764–2775. https://doi.org/10.1039/D2PY00271J.

- (32) Inal, S.; Rivnay, J.; Hofmann, A. I.; Uguz, I.; Mumtaz, M.; Katsigiannopoulos, D.; Brochon, C.; Cloutet, E.; Hadziioannou, G.; Malliaras, G. G. Organic Electrochemical Transistors Based on PEDOT with Different Anionic Polyelectrolyte Dopants. *J. Polym. Sci. Part B Polym. Phys.* **2016**, *54* (2), 147–151. https://doi.org/10.1002/polb.23938.
- (33) Inal, S.; Malliaras, G. G.; Rivnay, J. Benchmarking Organic Mixed Conductors for Transistors. *Nat. Commun.* **2017**, *8* (1), 1767. https://doi.org/10.1038/s41467-017-01812-w.
- (34) Solazzo, M.; Krukiewicz, K.; Zhussupbekova, A.; Fleischer, K.; Biggs, M. J.; Monaghan, M. G. PEDOT:PSS Interfaces Stabilised Using a PEGylated Crosslinker Yield Improved Conductivity and Biocompatibility. *J. Mater. Chem. B* **2019**, 7 (31), 4811–4820. https://doi.org/10.1039/C9TB01028A.
- (35) Kindaichi, S.; Matsubara, R.; Kubono, A.; Yamamoto, S.; Mitsuishi, M. Preparation of Resilient Organic Electrochemical Transistors Based on Blend Films with Flexible Crosslinkers. ChemRxiv April 25, 2023. https://doi.org/10.26434/chemrxiv-2023-zztqm.
- (36) Mantione, D.; del Agua, I.; Schaafsma, W.; ElMahmoudy, M.; Uguz, I.; Sanchez-Sanchez, A.; Sardon, H.; Castro, B.; Malliaras, G. G.; Mecerreyes, D. Low-Temperature Cross-Linking of PEDOT:PSS Films Using Divinylsulfone. *ACS Appl. Mater. Interfaces* **2017**, *9* (21), 18254–18262. https://doi.org/10.1021/acsami.7b02296.
- (37) Savva, A.; Saez, J.; Withers, A.; Barberio, C.; Stoeger, V.; Elias-Kirma, S.; Lu, Z.; Moysidou, C.-M.; Kallitsis, K.; Pitsalidis, C.; Owens, R. M. 3D Organic Bioelectronics for Electrical Monitoring of Human Adult Stem Cells. *Mater. Horiz.* **2023**. https://doi.org/10.1039/D3MH00785E.
- (38) Strakosas, X.; Sessolo, M.; Hama, A.; Rivnay, J.; Stavrinidou, E.; Malliaras, G. G.; Owens, R. M. A Facile Biofunctionalisation Route for Solution Processable Conducting Polymer Devices. *J. Mater. Chem. B* **2014**, *2* (17), 2537–2545. https://doi.org/10.1039/C3TB21491E.
- (39) Schüler, T.; Nykytenko, A.; Csaki, A.; Möller, R.; Fritzsche, W.; Popp, J. UV Cross-Linking of Unmodified DNA on Glass Surfaces. *Anal. Bioanal. Chem.* **2009**, *395* (4), 1097–1105. https://doi.org/10.1007/s00216-009-3045-9.
- (40) Xing, G.-W.; Xiang, S.; Xue, W.; Aodeng, G.-W.; Liu, Y.; Zhang, J.-H.; Lin, J.-M. Capture of Cervical Exfoliative Cells on a Glass Slide Coated by 3-Glycidyloxypropyl Trimethoxysilane and Poly-L-Lysine. *J. Pharm. Anal.* **2012**, *2* (3), 174–179. https://doi.org/10.1016/j.jpha.2012.02.008.
- (41) Wei, B.; Liu, J.; Ouyang, L.; Kuo, C.-C.; Martin, D. C. Significant Enhancement of PEDOT Thin Film Adhesion to Inorganic Solid Substrates with EDOT-Acid. *ACS Appl. Mater. Interfaces* **2015**, 7 (28), 15388–15394. https://doi.org/10.1021/acsami.5b03350.

- Ouyang, L.; Wei, B.; Kuo, C.; Pathak, S.; Farrell, B.; Martin, D. C. Enhanced PEDOT Adhesion on Solid Substrates with Electrografted P(EDOT-NH2). *Sci. Adv.* **2017**, *3* (3), e1600448. https://doi.org/10.1126/sciadv.1600448.
- Connell, L. S.; Gabrielli, L.; Mahony, O.; Russo, L.; Cipolla, L.; Jones, J. R. Functionalizing Natural Polymers with Alkoxysilane Coupling Agents: Reacting 3-Glycidoxypropyl Trimethoxysilane with Poly(γ-Glutamic Acid) and Gelatin. *Polym. Chem.* **2017**, 8 (6), 1095–1103. https://doi.org/10.1039/C6PY01425A.
- Zhang, S.; Kumar, P.; Nouas, A. S.; Fontaine, L.; Tang, H.; Cicoira, F. Solvent-Induced Changes in PEDOT:PSS Films for Organic Electrochemical Transistors. *APL Mater.* **2015**, *3* (1), 014911. https://doi.org/10.1063/1.4905154.
- (45) Shi, H.; Liu, C.; Jiang, Q.; Xu, J. Effective Approaches to Improve the Electrical Conductivity of PEDOT:PSS: A Review. *Adv. Electron. Mater.* **2015**, *I* (4), 1500017. https://doi.org/10.1002/aelm.201500017.
- (46) Koidis, C.; Logothetidis, S.; Kapnopoulos, C.; Karagiannidis, P. G.; Laskarakis, A.; Hastas, N. A. Substrate Treatment and Drying Conditions Effect on the Properties of Roll-to-Roll Gravure Printed PEDOT:PSS Thin Films. *Mater. Sci. Eng. B* 2011, 176 (19), 1556–1561. https://doi.org/10.1016/j.mseb.2011.03.007.
- (47) Lingstedt, L. V.; Ghittorelli, M.; Lu, H.; Koutsouras, D. A.; Marszalek, T.; Torricelli, F.; Crăciun, N. I.; Gkoupidenis, P.; Blom, P. W. M. Effect of DMSO Solvent Treatments on the Performance of PEDOT:PSS Based Organic Electrochemical Transistors. *Adv. Electron. Mater.* **2019**, *5* (3), 1800804. https://doi.org/10.1002/aelm.201800804.
- (48) Bernards, D. A.; Malliaras, G. G. Steady-State and Transient Behavior of Organic Electrochemical Transistors. *Adv. Funct. Mater.* **2007**, *17* (17), 3538–3544. https://doi.org/10.1002/adfm.200601239.
- (49) Khodagholy, D.; Rivnay, J.; Sessolo, M.; Gurfinkel, M.; Leleux, P.; Jimison, L. H.; Stavrinidou, E.; Herve, T.; Sanaur, S.; Owens, R. M.; Malliaras, G. G. High Transconductance Organic Electrochemical Transistors. *Nat. Commun.* **2013**, *4* (1), 2133. https://doi.org/10.1038/ncomms3133.
- (50) Ohayon, D.; Druet, V.; Inal, S. A Guide for the Characterization of Organic Electrochemical Transistors and Channel Materials. *Chem. Soc. Rev.* **2023**. https://doi.org/10.1039/D2CS00920J.
- Wu, H.-Y.; Yang, C.-Y.; Li, Q.; Kolhe, N. B.; Strakosas, X.; Stoeckel, M.-A.; Wu, Z.; Jin, W.; Savvakis, M.; Kroon, R.; Tu, D.; Woo, H. Y.; Berggren, M.; Jenekhe, S. A.; Fabiano, S. Influence of Molecular Weight on the Organic Electrochemical Transistor Performance of Ladder-Type Conjugated Polymers. *Adv. Mater.* 2022, 34 (4), 2106235. https://doi.org/10.1002/adma.202106235.

- (52) Stephen, M.; Wu, X.; Li, T.; Salim, T.; Hou, K.; Chen, S.; Leong, W. L. Crown Ether Enabled Enhancement of Ionic–Electronic Properties of PEDOT:PSS. *Mater. Horiz.* **2022**, *9* (9), 2408–2415. https://doi.org/10.1039/D2MH00496H.
- (53) Proctor, C. M.; Rivnay, J.; Malliaras, G. G. Understanding Volumetric Capacitance in Conducting Polymers. *J. Polym. Sci. Part B Polym. Phys.* **2016**, *54* (15), 1433–1436. https://doi.org/10.1002/polb.24038.
- (54) Keene, S. T.; Michaels, W.; Melianas, A.; Quill, T. J.; Fuller, E. J.; Giovannitti, A.; McCulloch, I.; Talin, A. A.; Tassone, C. J.; Qin, J.; Troisi, A.; Salleo, A. Efficient Electronic Tunneling Governs Transport in Conducting Polymer-Insulator Blends. *J. Am. Chem. Soc.* **2022**, *144* (23), 10368–10376. https://doi.org/10.1021/jacs.2c02139.
- (55) Keene, S. T.; Laulainen, J. E. M.; Pandya, R.; Moser, M.; Schnedermann, C.; Midgley, P. A.; McCulloch, I.; Rao, A.; Malliaras, G. G. Hole-Limited Electrochemical Doping in Conjugated Polymers. *Nat. Mater.* 2023, 22 (9), 1121–1127. https://doi.org/10.1038/s41563-023-01601-5.
- (56) Stavrinidou, E.; Leleux, P.; Rajaona, H.; Khodagholy, D.; Rivnay, J.; Lindau, M.; Sanaur, S.; Malliaras, G. G. Direct Measurement of Ion Mobility in a Conducting Polymer. *Adv. Mater.* **2013**, *25* (32), 4488–4493. https://doi.org/10.1002/adma.201301240.
- (57) de Izarra, A.; Park, S.; Lee, J.; Lansac, Y.; Jang, Y. H. Ionic Liquid Designed for PEDOT:PSS Conductivity Enhancement. *J. Am. Chem. Soc.* **2018**, *140* (16), 5375–5384. https://doi.org/10.1021/jacs.7b10306.
- (58) Greczynski, G.; Kugler, T.; Salaneck, W. R. Characterization of the PEDOT-PSS System by Means of X-Ray and Ultraviolet Photoelectron Spectroscopy. *Thin Solid Films* **1999**, 354 (1), 129–135. https://doi.org/10.1016/S0040-6090(99)00422-8.
- Zhang, Y.; Wang, Q.; Hu, F.; Wang, Y.; Wu, D.; Wang, R.; Duhm, S. Photoelectron Spectroscopy Reveals the Impact of Solvent Additives on Poly(3,4-Ethylenedioxythiophene):Poly(Styrenesulfonate) Thin Film Formation. *ACS Phys. Chem. Au* 2023. https://doi.org/10.1021/acsphyschemau.2c00073.
- (60) Bubnova, O.; Khan, Z. U.; Malti, A.; Braun, S.; Fahlman, M.; Berggren, M.; Crispin, X. Optimization of the Thermoelectric Figure of Merit in the Conducting Polymer Poly(3,4-Ethylenedioxythiophene). *Nat. Mater.* **2011**, *10* (6), 429–433. https://doi.org/10.1038/nmat3012.
- (61) Massonnet, N.; Carella, A.; Geyer, A. de; Faure-Vincent, J.; Simonato, J.-P. Metallic Behaviour of Acid Doped Highly Conductive Polymers. *Chem. Sci.* **2015**, *6* (1), 412–417. https://doi.org/10.1039/C4SC02463J.
- Won, D.; Kim, J.; Choi, J.; Kim, H.; Han, S.; Ha, I.; Bang, J.; Kim, K. K.; Lee, Y.; Kim, T.-S.; Park, J.-H.; Kim, C.-Y.; Ko, S. H. Digital Selective Transformation and Patterning of Highly Conductive Hydrogel Bioelectronics by Laser-Induced Phase Separation. *Sci. Adv.* **2022**, *8* (23), eabo3209. https://doi.org/10.1126/sciadv.abo3209.

- (63) Garreau, S.; Louarn, G.; Buisson, J. P.; Froyer, G.; Lefrant, S. In Situ Spectroelectrochemical Raman Studies of Poly(3,4-Ethylenedioxythiophene) (PEDT). *Macromolecules* **1999**, *32* (20), 6807–6812. https://doi.org/10.1021/ma9905674.
- (64) Chen, R.; Sun, K.; Zhang, Q.; Zhou, Y.; Li, M.; Sun, Y.; Wu, Z.; Wu, Y.; Li, X.; Xi, J.; Ma, C.; Zhang, Y.; Ouyang, J. Sequential Solution Polymerization of Poly(3,4-Ethylenedioxythiophene) Using V2O5 as Oxidant for Flexible Touch Sensors. *iScience* **2019**, *12*, 66–75. https://doi.org/10.1016/j.isci.2019.01.003.
- (65) Tan, E.; Pappa, A.-M.; Pitsalidis, C.; Nightingale, J.; Wood, S.; Castro, F. A.; Owens, R. M.; Kim, J.-S. A Highly Sensitive Molecular Structural Probe Applied to in Situ Biosensing of Metabolites Using PEDOT:PSS. *Biotechnol. Bioeng.* 2020, 117 (1), 291–299. https://doi.org/10.1002/bit.27187.
- (66) Duc, C.; Vlandas, A.; Malliaras, G. G.; Senez, V. Wettability of PEDOT:PSS Films. *Soft Matter* **2016**, *12* (23), 5146–5153. https://doi.org/10.1039/C6SM00599C.
- (67) Crispin, X.; Jakobsson, F. L. E.; Crispin, A.; Grim, P. C. M.; Andersson, P.; Volodin, A.; van Haesendonck, C.; Van der Auweraer, M.; Salaneck, W. R.; Berggren, M. The Origin of the High Conductivity of Poly(3,4-Ethylenedioxythiophene)–Poly(Styrenesulfonate) (PEDOT–PSS) Plastic Electrodes. *Chem. Mater.* **2006**, *18* (18), 4354–4360. https://doi.org/10.1021/cm061032+.
- (68) Mengistie, D. A.; Wang, P.-C.; Chu, C.-W. Effect of Molecular Weight of Additives on the Conductivity of PEDOT:PSS and Efficiency for ITO-Free Organic Solar Cells. *J. Mater. Chem. A* **2013**, *I* (34), 9907–9915. https://doi.org/10.1039/C3TA11726J.
- (69) Wang, Y.; Song, R.; Li, Y.; Shen, J. Understanding Tapping-Mode Atomic Force Microscopy Data on the Surface of Soft Block Copolymers. *Surf. Sci.* **2003**, *530* (3), 136–148. https://doi.org/10.1016/S0039-6028(03)00388-1.
- (70) Lang, U.; Müller, E.; Naujoks, N.; Dual, J. Microscopical Investigations of PEDOT:PSS Thin Films. *Adv. Funct. Mater.* **2009**, *19* (8), 1215–1220. https://doi.org/10.1002/adfm.200801258.
- (71) Jucius, D.; Lazauskas, A.; Grigaliūnas, V.; Gudaitis, R.; Guobienė, A.; Prosyčevas, I.; Abakevičienė, B.; Andrulevičius, M. Structure and Properties of Dual-Doped PEDOT:PSS Multilayer Films. *Mater. Res.* **2019**, *22*, e20190134. https://doi.org/10.1590/1980-5373-MR-2019-0134.
- (72) Menezes, N. P.; Nicolini, T.; Barker, M.; Mariano, A. A.; Dartora, C. A.; Wantz, G.; Stingelin, N.; Abbas, M.; Dautel, O. J.; Thuau, D. Improved Stability of Organic Electrochemical Transistor Performance with a Low Swelling Mixed Conducting Polymer: A Comparative Study with PEDOT:PSS. *J. Mater. Chem. C* **2023**, *11* (19), 6296–6300. https://doi.org/10.1039/D3TC00108C.

Table Of Contents (TOC) graphic

Same water and OECT stability

